In situ Observation of Adiabatic Shear Band Formation in Aluminum Alloys

Y. Nie[1], B. Claus[1], J. Gao[1], X. Zhai[1], N. Kedir[2], J. Chu[1], T. Sun[3], K. Fezzaa[3], W. W. Chen[1,2]

[1]*School of Aeronautics and Astronautics, Purdue University, West Lafayette, IN 47907, USA*
[2]*School of Materials Engineering, Purdue University, West Lafayette, IN 47907, USA*
[3]*Advanced Photon Source, Argonne National Laboratory, 9700 South Cass Avenue, Lemont, IL 60439, USA*

ABSTRACT

We used high-speed X-ray phase contrast imaging and infrared thermal imaging techniques to study the formation processes of adiabatic shear bands in aluminum 7075-T6 and 6061-T6 alloys. A modified compression Kolsky bar setup was used to apply the dynamic loading. A flat hat-shaped specimen design was adopted for generating the shear bands at the designated locations. Experimental results show that 7075-T6 exhibits less ductility and a narrower shear band than 6061-T6. Maximum temperatures of 720 K and 770 K were locally determined within the shear band zones for 7075-T6 and 6061-T6 respectively. This local high temperature zone and the resulting thermal instability were found to relate to the shear band formation in these aluminum alloys.

Introduction

When subject to dynamic loading, metals frequently exhibit localized shear deformation. This intense shearing is localized in a narrow band of highly deformed material, associated with local temperature rise resulting from plastic deformation accumulation over a short time, which is called an adiabatic shear band (ASB) [1]. The mechanism that results in shear band formation is considered as a local thermo-mechanical instability of the material. During plastic deformation, the plastic work is mainly converted into heat over a very short time period, leading to temperature increase within the material. If localized deformation at a high rate exists, thermal softening becomes locally significant. Under dynamic deformation, the heat dissipation is not fast enough and thermal softening will dominate over the effect of work hardening. Therefore, the deformation

becomes unstable and will grow within a narrow band forming the ASB [2]. Although an ASB is not a crack, it is closely related to the initiation of cracks and can further result in catastrophic material failure during dynamic loading. There are also applications where controlled shear bands are desired. Therefore, numerous efforts have been undertaken to determine the critical conditions under which ASB forms, as documented by reviews and books, such as Timothy [3], Xu *et al*. [4] and Dodd and Bai [5].

The formation of ASB has been found in many metals, including steel, titanium alloys, aluminum and aluminum alloys. The latter are widely used as structural materials in aerospace industries due to their light weight and design flexibility. Aluminum plates are also used in armor design as protective layers [6]. In these applications, the materials are commonly subjected to impact loading. The involved shear banding behavior can be a significant concern for structural integrity under dynamic loading conditions. Early experimental approaches regarding ASB formation were mostly focused on analyzing the specimens after shear band formation. Leech [7] confirmed the occurrence of ASBs in aluminum alloys during plate impact experiments. Owolabi *et al.* [8] performed dynamic compression experiments using a Kolsky bar apparatus on AA 6061 and compared the shear banding behavior with 6061/Al_2O_3 composites. The probability of ASB formation was found to increase when alumina was added as reinforcement. Li *et al*. [2] conducted impact experiments on AA 7075 with a thick-walled cylinder-external explosive collapse technique. The researchers examined the microstructure of post-mortem specimens and identified the deformed and the transformed shear bands.

Due to the difference in thermal and mechanical properties, materials exhibit different shear band propagation speed. These differences only have effect on a small region around a band tip. To better understand shear banding behavior and be able to predict shear band propagation, it is crucial to know not only the deformation, but also the temperature field around a propagating ASB tip. Hartley *et al*. [9] performed temperature measurements when loading tubular steel specimens with torsional Kolsky bar. They found a band width of 250 μm with a temperature rise of approximately 450 °C for low carbon steel. Duffy *et al*. [10] and Marchand and Duffy [11] reported real time measurement of strain using grid observation and temperature fields using an infrared camera. The alloy steels they studied exhibited shear bands roughly 20 μm in width. However, the spatial resolution for both temperature measurements were about the same as the width of the shear band, meaning the temperature measured was actually an average temperature around the band tip.

This average can be regarded as a lower bound of the local temperature peak. By tracking the temperature field, they were able to estimate an ASB propagation speed of ~500 m/s. Later, Zhou *et al*. [14] conducted an in-depth study on impacting notched C300 steel and Ti-6Al-4V. Both high-speed photography and temperature detection were used during the experiments. The maximum shear band speed of steel was found to be 1200 m/s and was strongly dependent on the impact velocity. The maximum temperature rise was approaching 1400 °C for C300 steel at an impact velocity of 43 m/s, while only 450 °C for Ti-6Al-4V at an impact velocity of 64.5 m/s. Based on the experimental findings, Mercier and Molinari [15] proposed an analytical model to describe the dynamic ASB propagation in mode II. In contrast to the shear band formation studies on steel and titanium alloys, temperature measurements on aluminum alloys are rarely reported. Hence, studies on the conditions under which shear bands initiate and propagate as well as the evolution of temperature fields within the shear bands are required for determining the structural integrity of aluminum alloys under dynamic loading conditions.

Guduru *et al*. [14] also investigated the strain and temperature fields in a fully developed ASB of C300 steel, but with the coherent gradient sensing technique and a self-developed high-speed infrared camera. The results showed a non-uniform temperature distribution along the shear band. Multiple high temperature areas were observed with the spacing in the range of 0.25 mm to 1 mm. The high-speed infrared camera technique provided a possibility for measuring the temperature rise with higher spatial and temporal resolutions. More recently, Guo *et al.* [15] reported shear banding experiments on commercial titanium using a compression Kolsky bar setup with both high-speed camera and infrared camera. The group of researchers claimed the temperature rise in the titanium occurs after ASB formation, which is considered to be the consequence of ASB. This result raised a new concern towards the relationship between the mechanical and thermal behaviors of shear banding.

Despite these efforts, the best spatial resolution of the aforementioned deformation measurements was only in the order of tens of microns. Observation of ASB propagation in real time with higher resolution is still desired to pinpoint the critical conditions. Considering that the width of ASB reported in the literature is mainly in the order of 10^0 to 10^2 μm and the shear band speed can reach several thousand meters per second, a visualization method with both higher spatial resolution and higher frame rate is desired to better observe the local shear band propagation and locate the propagating band tip. However, it is challenging to further improve the spatial

resolution. This is partially limited by the wave length of visible light and the short working distance from the specimen when a high magnification lens is used. An experimental technique has recently been introduced by Hudspeth *et al*. [16] where a Kolsky bar setup is synchronized with high-speed synchrotron X-ray imaging at Argonne National Laboratory. The technique incorporating X-ray Phase Contrast Imaging (X-ray PCI) was developed to capture the damage history during a dynamic experiment in real time. Parab *et al*. [17] utilized this technique to observe the crack propagation in glass and showed the possibility for *in situ* observation of damage development inside certain opaque materials under dynamic loading. A spatial resolution of 1.6 μm can be achieved by using a magnification of 20× with a sufficient objective distance depending on the location of the scintillator. The temporal resolution can be at 200 ns or 5 million frames per second. This method offers a new opportunity in observing the initiation and propagation of an ASB in more details.

Materials and Methods

Material and specimen

The focus of this study is to examine the effectiveness of using high-speed X-ray PCI and high-speed thermal imaging to investigate ABS in metals. The materials used in this study were selected to be well-studied commercially available aluminum alloys 7075-T6 and 6061-T6. In order to image the shear band formation at a pre-determined location, a hat-shaped specimen geometry was adopted. This hat-shaped specimen method, introduced by Meyer *et al.* [18] and Hartmann *et al.* [19], has been widely used to study the shear localization of various metals [20-23]. The advantage of using this geometry is that shear bands can be generated in many ductile materials within the designated narrow region [24]. The versatility of the specimen geometry design enables precise control over the desired stress state with a conventional compression Kolsky bar setup. The deformation in the specimens can also be easily stopped at desired stages by having stoppers with proper thickness to collect the specimen before fracture.

Most of the hat-shaped specimens in previous research were designed in a cylindrical shape like a real “hat”. However, in this work, a flat hat-shaped specimen with thickness of 0.8 mm is used to facilitate *in situ* high-speed X-ray visualization. The specimen geometry is shown in Fig. 1 and

the dimensions are presented in Table 1. The punch width w_1 is designed to be larger than the opening width w_2 to achieve a compression-shear stress state. This stress state prevents the material from experiencing early failure so that the adiabatic shearing can be visualized.

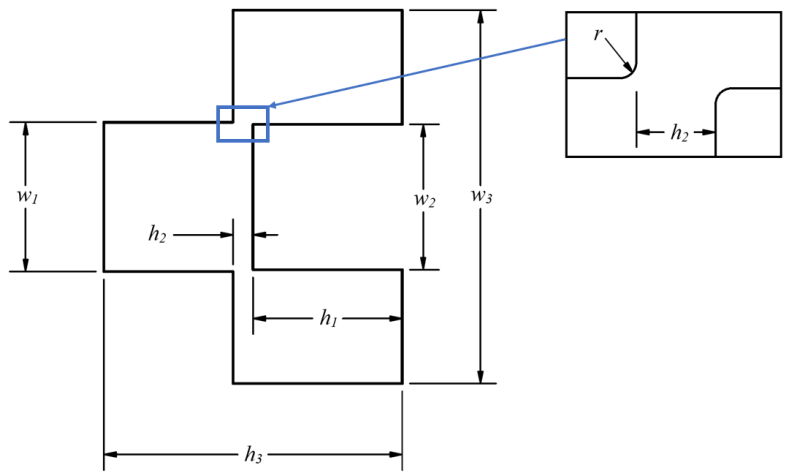

Fig. 1. The geometry of hat-shaped specimen and the compression-shear region

Table 1 Dimensions of the hat-shaped specimen shown in Fig. 1 (mm)

w_1	w_2	w_3	h_1	h_2	h_3	r
7.62	7.42	19.05	7.62	1.02	15.24	0.25

The specimens were cut to dimensions from aluminum sheets with wire electrical discharge machining (EDM) to minimize the damage on the edges of the specimens. Then multiple vertical lines were carved within the compression-shear region of the specimens by a razor blade, providing sufficient contrast to reveal the localized shear deformation in the material. Because of the nature of the specimen dimension, plane stress condition is assumed so that the material is considered to be uniformly deformed through the thickness and only the surface deformation is measured.

Experimental techniques

The dynamic experiments with X-ray PCI were performed at beamline 32-ID-B of the Advance Photon Source (APS) at Argonne National Laboratory. A compression Kolsky bar integrated with

the synchrotron X-ray imaging setup was developed through collaboration between Purdue University and APS. A schematic of the experimental setup is presented in Fig. 2. This method was discussed in more detail in [16].

When an experiment starts, the striker is launched pneumatically to impact the incident bar (Fig. 2). A compressive stress pulse is then generated and propagates along the incident bar from the impact side towards the specimen. The pulse is recorded by the oscilloscope through a pair of strain gages and helps to trigger the high-speed camera. When the stress pulse reaches the bar end, the specimen is loaded at the same impact velocity as the striker. The *in-situ* shear banding and crack propagation were recorded at 5 MHz frame rate with a Shimadzu HPV-X2 high-speed camera. Appropriate time delays need to be calibrated prior to the experiments to synchronize the camera with the start of the loading and passing of the X-rays through the specimen to capture the dynamic shear band forming event. A specimen holder is designed to support the specimen in position and prevent buckling, as shown in Fig. 3. The material deformation and shear banding are captured by a scintillator-camera system while the dynamic force history is recorded by a piezoelectric load cell (Kistler 9212). For the experiments reported in this paper, striking velocities were 16 ± 2 m/s.

The temperature field measurements during the dynamic shearing event were performed separately with the same compression Kolsky bar setup. The experimental conditions were maintained the same so that the results can be directly related to the X-ray imaging experiments. A Telops FastM3k infrared thermal camera with 1× lens was used to record the surface temperature distribution of the aluminum specimens at 64 kHz. The view window of the thermal camera is 1.6×0.4 mm and the pixel size of the image is 30 μm. A photograph of the experimental setup is shown in Fig. 4. The thermal camera was pre-calibrated with a black body by the manufacturer before being used in this work. During the experiments, the lens of the camera is adjusted to focus on the surface of the specimen.

The true temperature is calculated from the radiance temperature with the equation below:

$$T_{true} = \frac{T_{rad}}{\sqrt[4]{\varepsilon}} \tag{1}$$

where ε is the emissivity of the given material. Wen and Mudawar [25] performed an independent study on the emissivity of various aluminum alloys with different surface quality, temperature

ranges and wavelength ranges. The results show that the emissivity of a certain aluminum alloy does not change significantly in 3 – 5 μm wavelength range and 600 – 800 K temperature range, which are our application ranges. The aluminum specimens used in this work were initially mirror polished, but due to exposure to air they quickly formed a visible oxide layer. During deformation, the material surface can gradually become rough, which leads to the change of the emissivity within 0.1 – 0.2. Fig. 5 shows the relationship between true temperature calculated by equation (1) and emissivity, given the radiance temperature of 450 K and 480 K. When the emissivity varies between 0.1 and 0.2, there will be approximately 10% error in the calculated true temperature. Taking all the aforementioned factors into account, an averaged constant emissivity of 0.15 is used for both aluminum alloys in this paper.

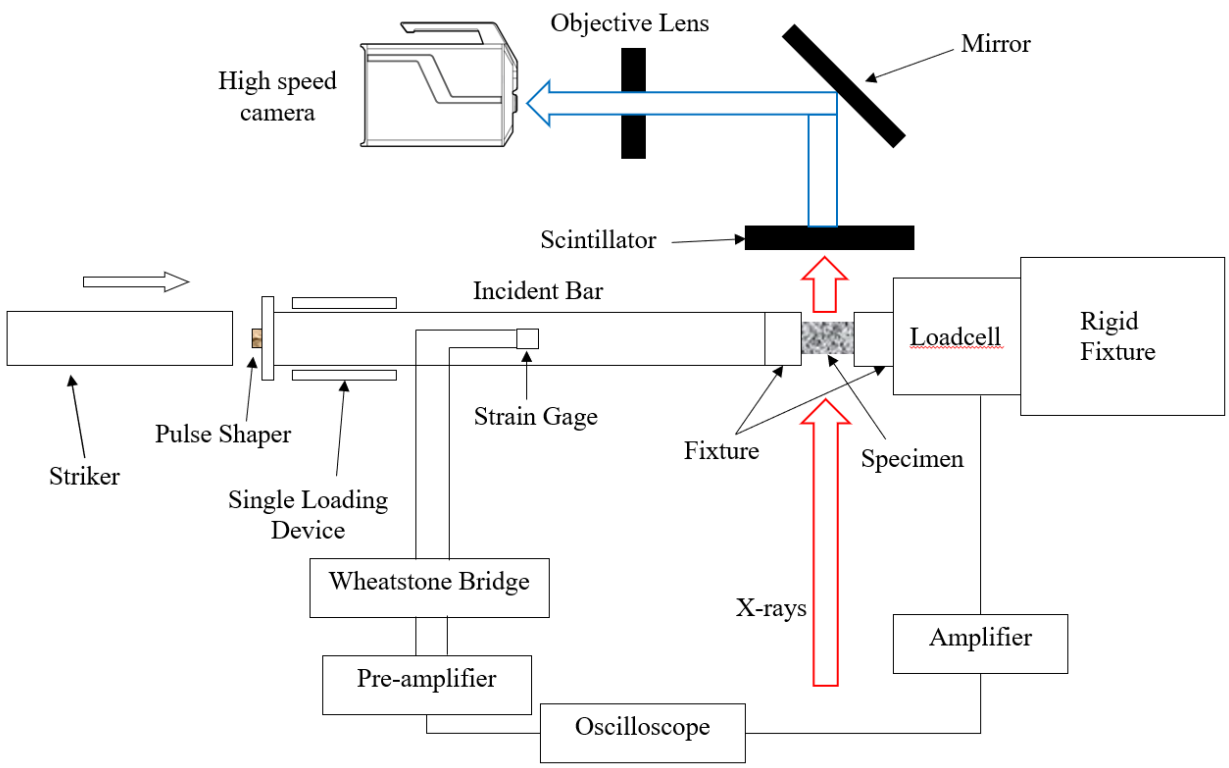

Fig. 2. Dynamic compression setup with high-speed X-ray phase contrast imaging

Fig. 3. A photograph of the specimen section of the Kolsky bar setup

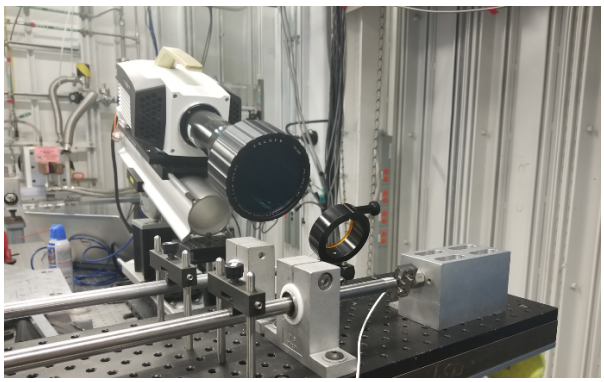

Fig. 4. A photograph of experimental setup of high-speed infrared camera and Kolsky bar.

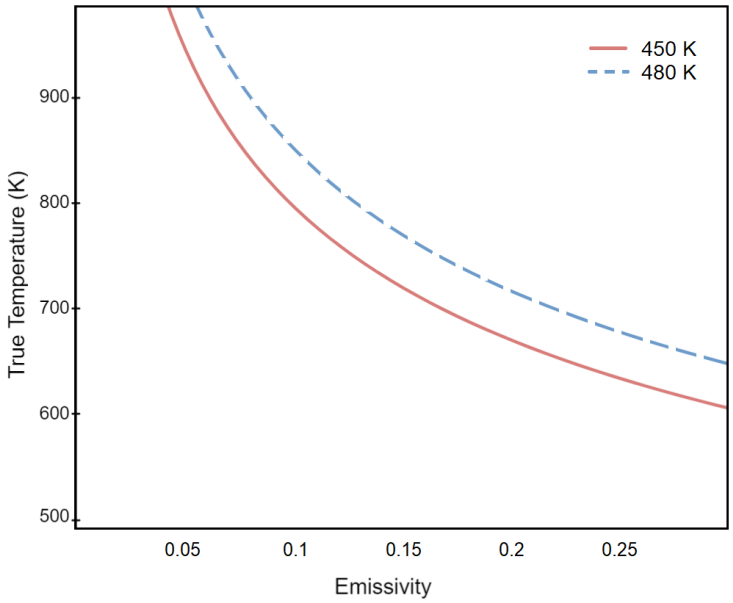

Fig. 5. The true temperature–emissivity relationships at radiance temperature of 450 K and 480 K.

Experimental Results

Aluminum 7075-T6

The shear banding behaviors of the aluminum 7075-T6 under dynamic shear were studied in five hat-shaped specimens under repeated experimental conditions. The force-displacement relationship and the high-speed image sequence of a representative experiment are shown in Fig. 6. An edge detection algorithm with polynomial curve fit is used to track the deformation of the blade carved lines from image 2 to 6. The gradient of these computer-generated lines represents the shear strain. When the hat-shaped specimen is compressed, the material in the desired shear region is subject to shear. The carved lines bend during the deformation and the distortion is most significant in the area where the maximum shear strain is located. By tracking the movement of the lines and calculating the gradients of the fitted curves, the approximate strain can be obtained, which is corresponding to the time sequence of the images. When the value of the maximum derivative along a line exceed 1.0, we consider a shear band formed. The points when the high-speed images were taken are marked on the force history plot.

In this particular experiment, the camera window is focus on the area that is shown in the close-up view in Fig. 1. One of the corner edges of the specimen is just outside the left side of the camera imaging window of 0.64 mm by 0.4 mm. At t = 0 μs, the specimen starts being loaded. All of the razer-blade-carved parallel lines remain straight, showing no deformation in the material. At t = 16.8 μs, shear deformation can be observed within the designated gage section. However, by taking a close examination of the line gradients, we can find that the first line from the left has larger gradient than the other lines. The maximum local shear strain along this line is measured as 1.4, which indicates that the dynamic shear deformation is propagating along the loading direction, i.e., from left to right in the image. This shear deformation then becomes highly localized and starts to form a shear band in the image taken at t = 17.4 μs. At t = 18 μs, the maximum shear strains along the six lines range from 1.9 to 5.7. A crack initiation is also oberved, as marked by the arrow. This crack propagates along the same direction as the ASB (t = 18.6 μs), resulting in the discontinuity of the left two vertical lines. In this experiment, the force approaches its maximum at this point. But in some other experiments, the force was found to keep increasing after the shear band is initiated. This can be caused by the specimen geometry.

There are two shear regions on each specimen and which one fails first is random. At t = 19.2

μs, the crack causes the material to separate. The crack speed can be estimated from the images as ~1100 m/s. The entire fracture of the specimen occurs when the crack propagates through the gage section, which is not recorded in these images. During the entire recorded event, no significant shear strain is found in the vertical direction, as the horizontal carved lines remain straight in all six images.

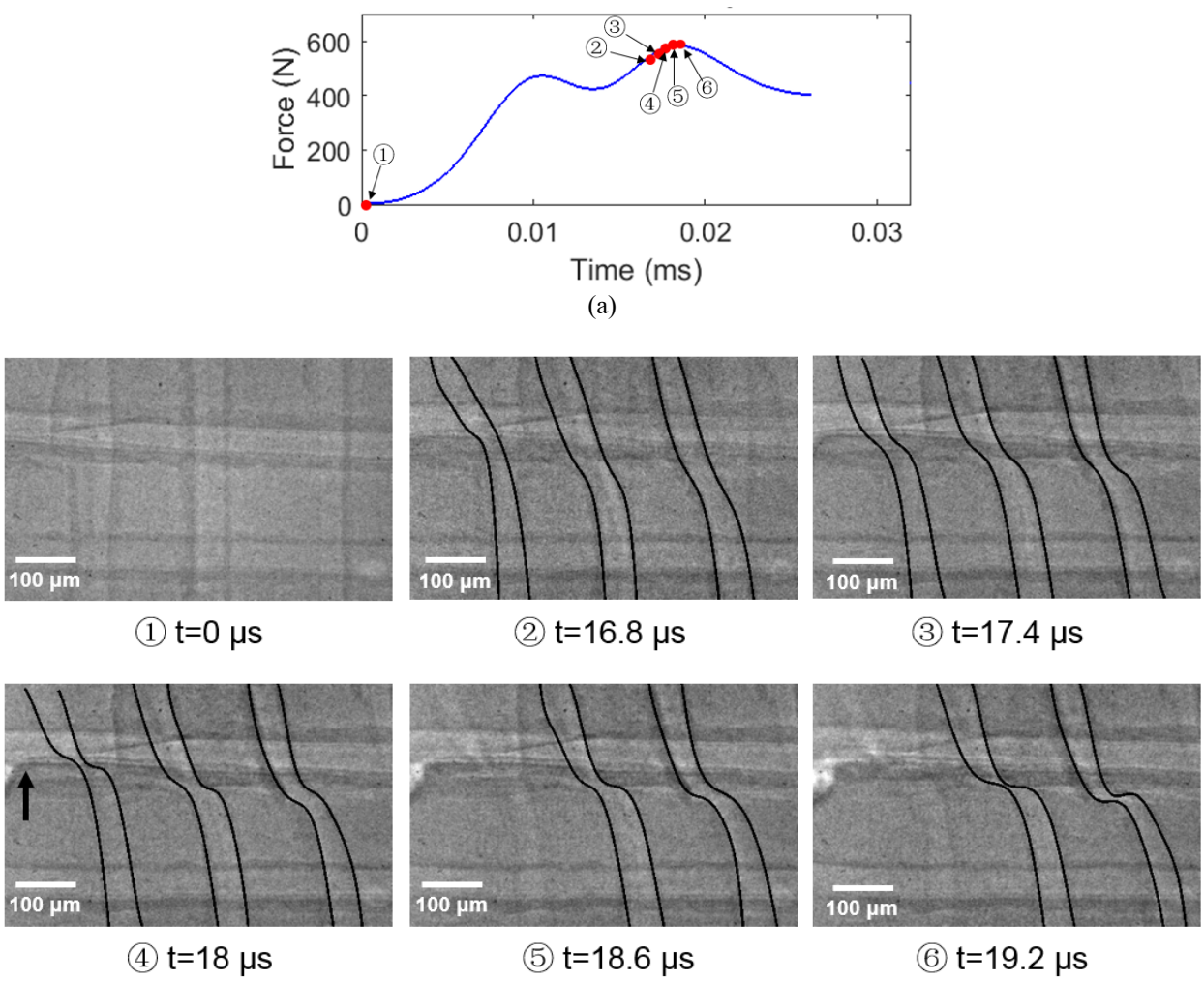

Fig. 6. The force-time graph (a) and the corresponding image sequence (b) of a representative dynamic shear experiment on aluminum 7075-T6. Lines are tracked and marked to show the shear deformation.

The temperature field measurements on aluminum 7075-T6 during the dynamic shear were performed without X-ray PCI. The high-speed infrared camera measured the sample temperature

from the direction perpendicular to the sample plane and the loading direction. The experimental conditions were identical to the experiments as shown in Fig. 6. The results on the temperature field evolution on the shear band are shown in Fig. 7. Due to the limitation in the frame rate, only two to three images are captured during the loading phase. The loading begins at t = 0 μs. At t = 16 μs, a thin band of temperature increase can be observed initiating from both edges of the specimen due to the shear deformation. The temperature is approximately 450 K along the region. At t = 31 μs, the image shows a peak temperature of 720 K in the center of the gage section. From Fig. 6 we know that the shear band has already formed at this strain level. Therefore, even though the number of thermal image frames is still limited, the images in Figures 6 and 7 indicate that the shear bands initiate from both edges, propagate towards each other, and meet at the center, where the peak temperature is captured. At t = 47 μs, the high temperature zone has split into two in the vertical direction, which indicates that the material has separated across the shear band. The force history also shows the material has already failed at this time. The residual heat requires time to dissipate into the material, which results in a gradually decreasing temperature and a shrinking zone in the last two images, when the force has already reached zero.

The thermal experiments are repeated four times, whereas, as mentioned earlier, the X-ray imaging experiments on aluminum 7075-T6 are repeated five times. The force-displacement behaviors for the experiments are presented in Fig. 8. Although the graph shows a scatter of ~20%, all the results show a similar trend. The shear bands initiate when the displacement is approximately 0.2 mm, where the force has not reached the maximum. The observed failure modes are consistent among all the experiments. For the temperature field measurements, the images are not directly comparable with the X-ray images, since the time when recording starts varies from each experiment and the images are captured at different time frame during the loading. However, all the results indicate the same band width of ~100 μm in which the temperature is over 600 K.

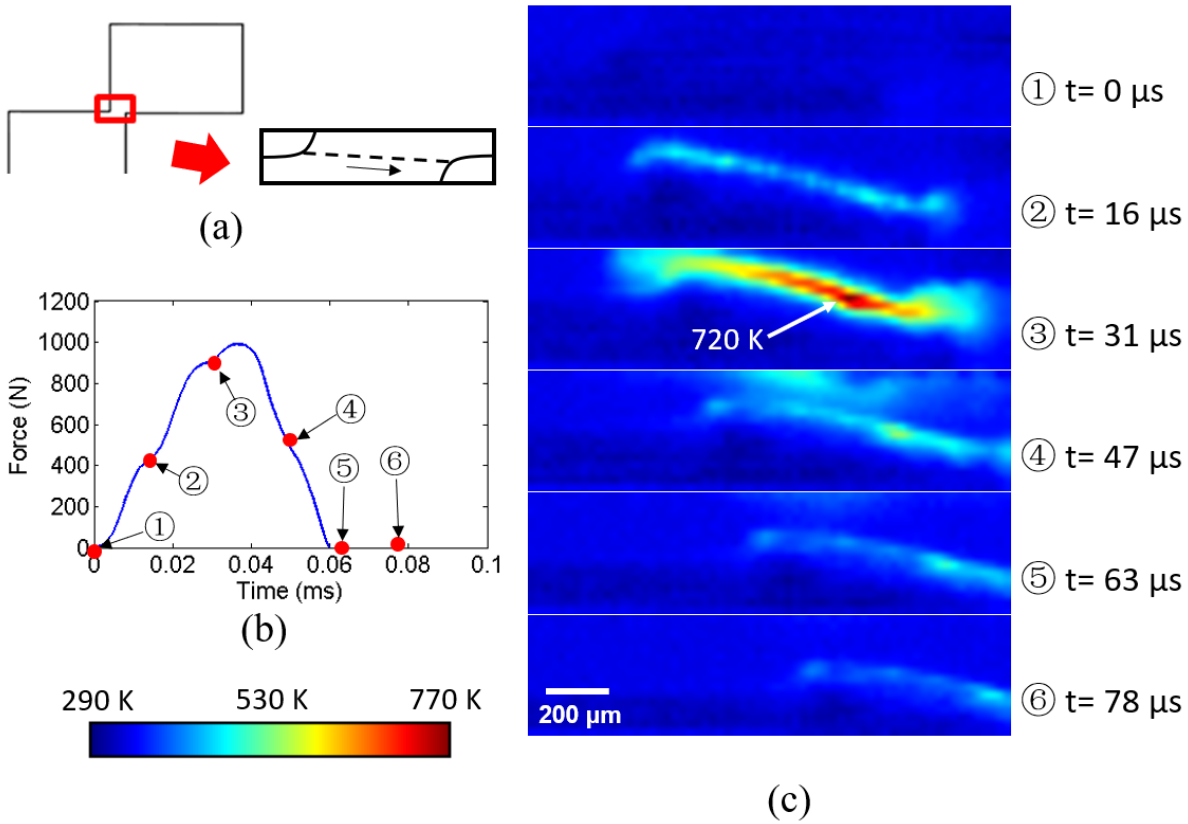

Fig. 7. A representative force-time relationship and the corresponding thermal image sequences of aluminum 7075-T6. (a) The location of the camera window. (b) The force-time graph. (c) The thermal image sequence showing the temperature field on the material surface.

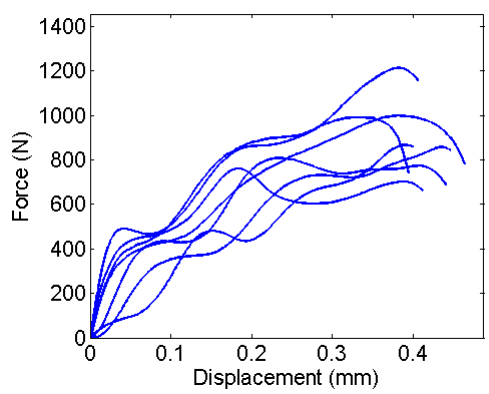

Fig. 8. The force-displacement curves of aluminum 7075-T6.

Aluminum 6061-T6

Experiments under identical conditions were conducted on aluminum 6061-T6 to compare the material properties with 7075-T6. The force-displacement relationship and the high-speed image sequence of a representative experiment are presented in Fig. 9. When loading starts, the specimen first adjust itself for better contact with the bar end and the fixture. At t = 16.4 μs, the material deforms uniformly and the maximum shear strains along all lines are measured as approximately 0.9. At t = 17.8 μs, the shear deformation becomes localized along the left two lines, showing the shear strain of 1.4. When loading continues, the shear band can be clearly seen initiating from the left side referring to the razor-blade carved grooves (t=19.2 μs). At t = 20.4 μs, the shear band is horizontal in the lower area of the image, with the average maximum shear strain of 3.2 along the band. A crack also initiates from the location indicated with an arrow. This crack later propagates along the shear direction (t = 21.6 μs). The force reaches a small plateau at this point, but has not reached the maximum of the entire loading history. Similar to the experiments with 7075-T6, no significant shear deformation is found in vertical direction according to the straight horizontal lines in all six images.

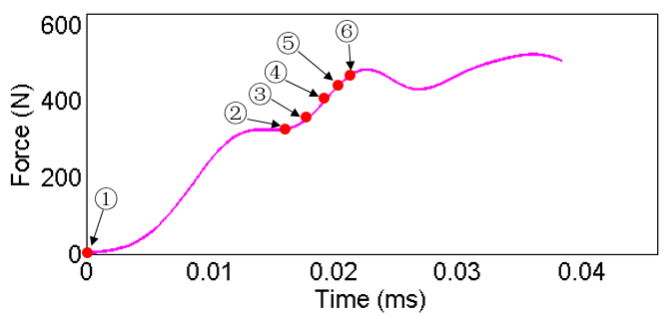

(a)

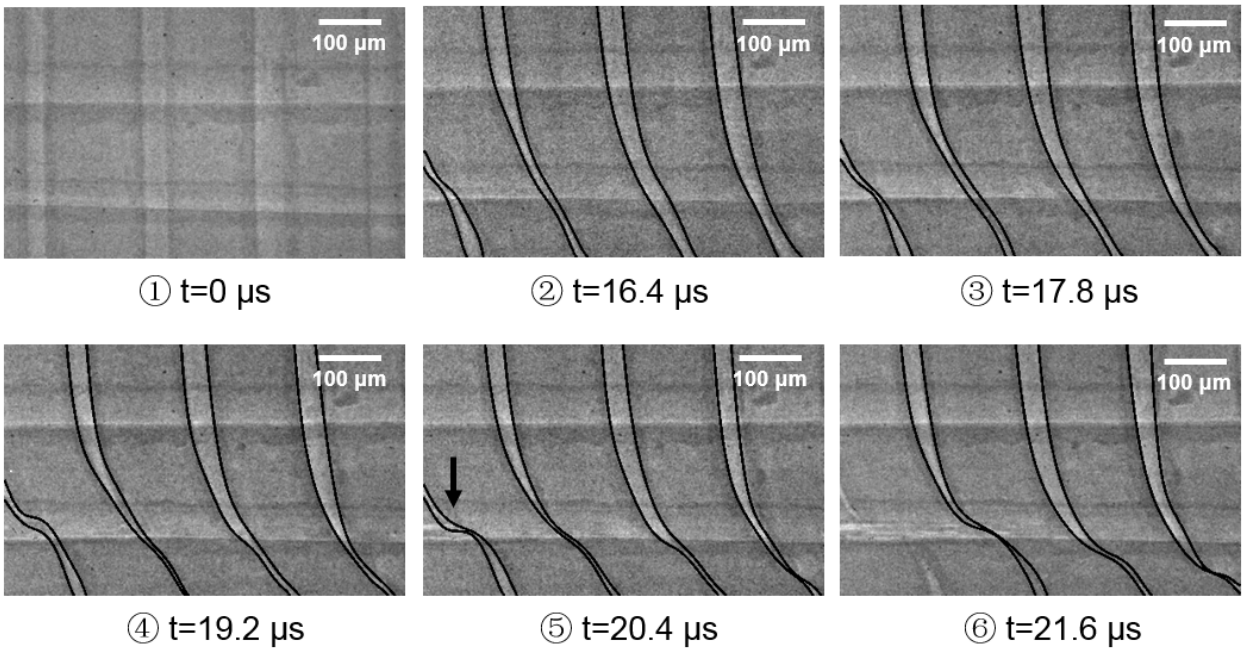

(b)

Fig. 9. (a) The force-time graph and (b) the corresponding image sequence of a representative dynamic shear experiment on aluminum 6061-T6. Lines are tracked and marked to show the shear deformation.

The infrared thermal imaging results of 6061-T6 are arranged in Fig. 10. The compression loading begins at t = 0 μs. At t =16 μs, there emerge two high temperature zones from both edges of the specimen with almost the same temperature of around 600 K. These two peaks propagate towards each other and become closer at t = 31 μs. This observation again reveals the processes of shear band formation and propagation. The calculated temperature also reaches a maximum of 770 K where the two tips meet. Then at t = 47 μs, the force reaches the maximum and the material fails. The heat can be seen gradually dissipating to the adjacent regions in the last 4 images. The lower part of the specimen is pushed out of the window by the incident bar.

Note that only one representative experimental result of aluminum 6061-T6 from five repeated experiments is presented here. The force-displacement curves are shown in Fig. 11, which show good repeatability among the results. The measured temperature fields were also consistent across the repeated experiments. The highest calculated temperature is in the range of 600 K to 770 K and the band width is ~160 μm in which the temperature is over 600 K.

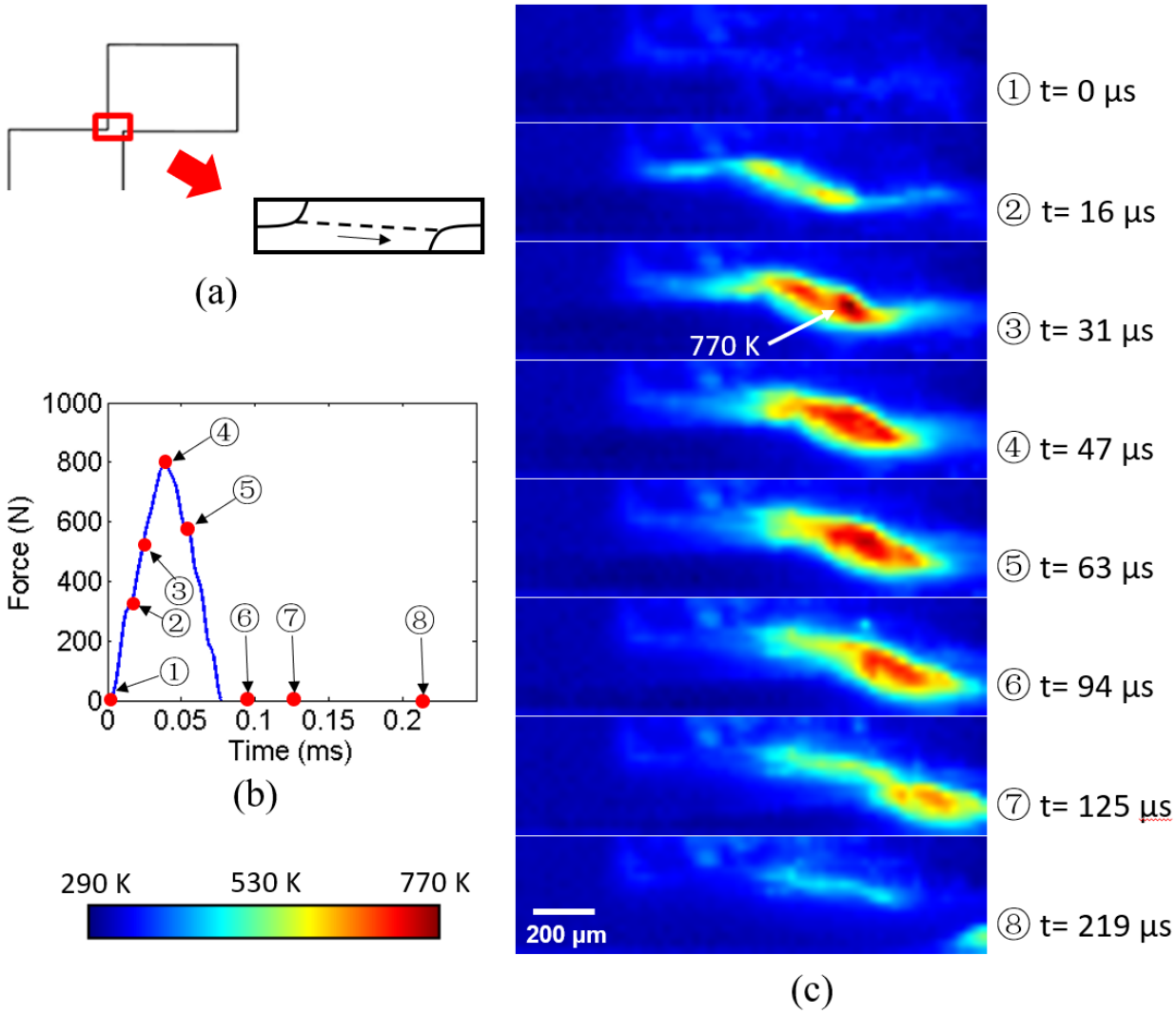

Fig. 10. A representative force-time relationship and the corresponding thermal image sequences of aluminum 6061-T6. (a) The location of the camera window. (b) The force-time graph. (c) The thermal image sequence showing the temperature field on the material surface.

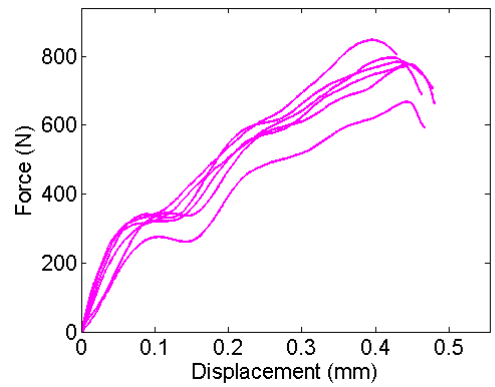

Fig. 11. The force-displacement curves of aluminum 6061-T6.

Discussion

In order to estimate the thermal conduction near the localized shear zone, the temperature in the shear band can be assumed uniform. Therefore heat diffusion is only considered in the normal direction away from the shear band. The condition is then simplified as one-dimensional. The simplified heat equation is given as

$$\alpha \frac{\partial^2 T}{\partial x^2} = \frac{\partial T}{\partial t} \tag{2}$$

where T is the temperature and α is the thermal diffusivity of the material. For the aluminum 7075-T6, the thermal diffusivity is reported to vary from 0.65 to 0.75 cm^2/s when temperature is changing from 300 K to 800 K [26]. Here α is chosen as 0.7 cm^2/s. Similarly, α can be estimated as 0.75 cm^2/s for aluminum 6061-T6. To simulate the case where the shear band has been fully developed, the boundary condition is taken as infinite long solid with no heat generation inside. Considering the extreme case that the temperature is initially equal to the peak temperature found in the infrared experimental results, the heat equation has the following solution:

$$T(x,t) = T_s + \frac{T_0 - T_s}{2\sqrt{\alpha \pi t}} \int_{-1}^{1} \exp\left[-\frac{(x-d)^2}{4\alpha t} \right] du \tag{3}$$

where T_0 is the peak temperature, T_s is room temperature and d is the half shear band width. Figures 12 and 13 show the heat distribution within 7075-T6. Although it is initially room temperature

outside the shear band, the heat conduction to the adjacent area is negligible given that the shear band formation takes less than 100 μs. Therefore the adiabatic condition applies. The result for 6061-T6 is very similar since the material properties and peak temperature are close to those for 7075-T6. The temperature dependence is discussed in [1] that the material will show lower stress in adiabatic condition than in isothermal condition. Given temperature rise close to the material melting temperature, the material is considered to undergo significant thermal softening.

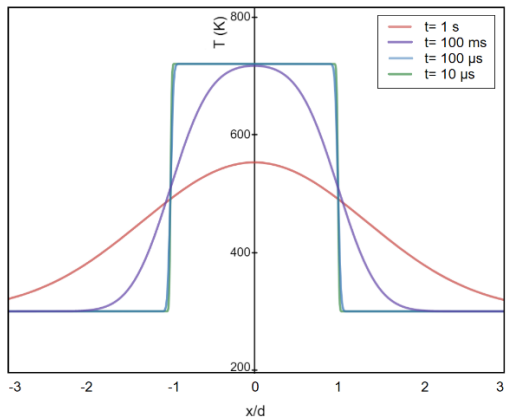

Fig. 12. Temperature distribution in aluminum 7075-T6 at different time after the adiabatic shear band formation. *d* is half of the shear band width.

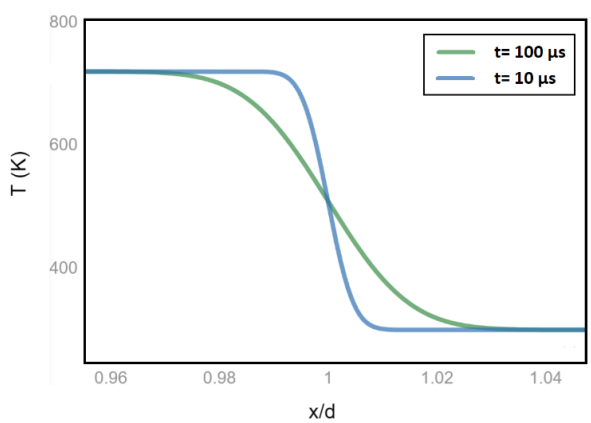

Fig. 13. A detailed view of the temperature distribution in aluminum 7075-T6 at 10 μs and 100 μs after the adiabatic shear band formation. *d* is half of the shear band width.

Both 7075-T6 and 6061-T6 show shear banding behaviors and similar temperature response. Based on the high-speed X-ray images, 7075 is found to be more brittle than 6061 under dynamic shear. In 7075, the shear bands and cracks initiate shortly after localized shear deformation is present, while 6061 exhibit larger shear strain than 7075 when the shear band forms. The shear

banding behaviors are found before the force reaches the maximum. These findings are in accordance with the thermal images, where 7075 has a peak temperature at t=31 μs and 6061 still has two peaks propagating in the same time frame. By correlating the timing of X-ray and thermal images for both aluminum alloys, the temperature can be shown to reach peak values after the observation of shear bands, which is considered to be the result of the insufficient thermal camera frame rate. Considering the nature that the events of maximum temperature and shear band formation are very close to each other, a higher frame rate for temperature measurement is desired to determine the exact time of the temperature rise.

Both aluminum alloys reach very high temperature during the dynamic loading with 720 K for 7075 and 770 K for 6061. As shown in Fig. 5, the emissivity is taken as a constant of 0.15. Considering that the melting point for 7075-T6 is approximately 750 K and 850 K for 6061-T6, the materials were locally close to melting status. The difference in melting points can also be a reason that 7075 showed lower overall temperature response than 6061. The shear band width is also an important quantity to study. However, both materials exhibit very narrow ASB. The precise measurement is difficult due to the limit of the spatial resolution. Based on the presented X-ray and thermal images, the shear band width can be safely estimated as 20-50 μm for 7075-T6 and 30-70 μm for 6061-T6 before cracks form. Since the formation of the shear band takes less than 100 μs, the thermal conduction length can be found to be 0.01 – 0.02 of the half shear band width *d*, according to Fig. 13. The thermal conduction length is in the order of 10^2 nm. This thermal conduction length is so small that the material inside the shear band is considered to be in adiabatic condition. The induced strain softening makes the material locally weaker than the adjacent area that are unaffected by the temperature rise. Therefore the deformation is concentrated within this localized region, forming the adiabatic shear band.

Conclusion

Aluminum 7075-T6 and 6061-T6 were studied in this paper under dynamic shear loading. The flat hat-shaped specimen geometry was adopted with an impact speed of ~16 m/s. Both materials presented the trend of uniform shear deformation, formation of shear bands, cracking and then shear failure. 6061-T6 is more ductile and requires larger strain to form ASB. The temperature fields were measured using a high-speed infrared thermal camera. By assuming the emissivity to

be 0.15, the maximum temperature during the loading was found to be 720 K for 7075-T6 and 770 K for 6061-T6. This heat accumulation and the corresponding thermal instability during dynamic loading were found to be closely related to the formation of the ASB. Both X-ray and thermal imaging in this research give useful information in determining the shear band width and tip location. The shear band width is estimated as 20-50 μm for 7075-T6 and 30-70 μm for 6061-T6. The cracks initiate after shear bands form and propagate in the same tracks as the shear bands at approximately 1100 m/s.

Acknowledgements

This material is based upon work supported in part by the U. S. Army Research Laboratory and the U. S. Army Research Office under grant number W911NF1710241. The authors also sincerely thank Alex Deriy at the APS for his professional help during our beam time, and Aaron Greco at Argonne for his cooperation in using the IR camera. This research used resources of the Advanced Photon Source, a US Department of Energy (DOE) Office of Science User Facility operated for the DOE Office of Science by Argonne National Laboratory under Contract No. DE-AC02-06CH11357. Funding for high-speed camera used in this work was provided by AFOSR Award No. FA9550-16-1-0315 (Dr. Martin Schmidt, Program Officer).

References

[1] Zener, Clarence, and John Herbert Hollomon. "Effect of strain rate upon plastic flow of steel." Journal of Applied physics 15.1 (1944): 22-32.

[2] Li, D. H., Y. Yang, T. Xu, H. G. Zheng, Q. S. Zhu, and Q. M. Zhang. "Observation of the microstructure in the adiabatic shear band of 7075 aluminum alloy." Materials Science and Engineering: A 527, no. 15 (2010): 3529-3535.

[3] Timothy, S. P. "The structure of adiabatic shear bands in metals: a critical review." Acta Metallurgica 35.2 (1987): 301-306.

[4] Xu, Y., Jinghua Zhang, Yilong Bai, and Marc Andre Meyers. "Shear localization in dynamic deformation: microstructural evolution." Metallurgical and materials transactions A 39, no. 4 (2008): 811.

[5] Dodd, Bradley, and Yilong Bai, eds. Adiabatic shear localization: frontiers and advances. Elsevier, 2012.

[6] Luz, Fernanda Santos da, Lima Junior, Edio Pereira, Luis Henrique Leme Louro, and Sergio Neves Monteiro. "Ballistic test of multilayered armor with intermediate epoxy composite reinforced with jute fabric." Materials Research 18 (2015): 170-177.

[7] Leech, Patrick W. "Observations of adiabatic shear band formation in 7039 aluminum alloy." Metallurgical transactions A 16.10 (1985): 1900-1903.

[8] Owolabi, G. M., A. G. Odeshi, M. N. K. Singh, and M. N. Bassim. "Dynamic shear band formation in Aluminum 6061-T6 and Aluminum 6061-T6/Al2O3 composites." Materials Science and Engineering: A 457, no. 1-2 (2007): 114-119.

[9] Hartley, K. A., J. Duffy, and R. H. Hawley. Measurement of the temperature profile during shear band formation in steels deforming at high strain rates. BROWN UNIV PROVIDENCE RI DIV OF ENGINEERING, 1986.

[10] Duffy, J., and Y. C. Chi. "On the measurement of local strain and temperature during the formation of adiabatic shear bands." Materials Science and Engineering: A 157.2 (1992): 195-210.

[11] Marchand, A., and J. Duffy. "An experimental study of the formation process of adiabatic shear bands in a structural steel." Journal of the Mechanics and Physics of Solids 36.3 (1988): 251-283.

[12] Zhou, M., A. J. Rosakis, and G. Ravichandran. "Dynamically propagating shear bands in impact-loaded prenotched plates—I. Experimental investigations of temperature signatures and propagation speed." Journal of the Mechanics and Physics of Solids 44.6 (1996): 981-1006.

[13] Mercier, S., and A. Molinari. "Steady-state shear band propagation under dynamic conditions." Journal of the Mechanics and Physics of Solids 46.8 (1998): 1463-1495.

[14] Guduru, P. R., A. J. Rosakis, and G. Ravichandran. "Dynamic shear bands: an investigation using high speed optical and infrared diagnostics." Mechanics of Materials 33.7 (2001): 371-402.

[15] Guo, Yazhou, Qichao Ruan, Shengxin Zhu, Q. Wei, Haosen Chen, Jianan Lu, Bo Hu, Xihui Wu, Yulong Li, and Daining Fang. "Temperature Rise Associated with Adiabatic Shear Band: Causality Clarified." Physical Review Letters 122.1 (2019): 015503.

[16] Hudspeth, M., B. Claus, S. Dubelman, J. Black, A. Mondal, N. Parab, C. Funnell, F. Hai, M.L. Qi, K. Fezzaa, S.N. Luo. "High speed synchrotron X-ray phase contrast imaging of dynamic material response to split Hopkinson bar loading." Review of Scientific Instruments 84.2 (2013): 025102.

[17] Parab, Niranjan D., John T. Black, Benjamin Claus, Matthew Hudspeth, Jianzhuo Sun, Kamel Fezzaa, and Weinong W. Chen. "Observation of Crack Propagation in Glass Using X-ray Phase Contrast Imaging." International Journal of Applied Glass Science 5.4 (2014): 363-373.

[18] Meyer, L. W., E. Staskewitsch, and A. Burblies. "Adiabatic shear failure under biaxial dynamic compression/shear loading." Mechanics of Materials 17.2-3 (1994): 203-214.

[19] Hartmann, K-H., H-D. Kunze, and L. W. Meyer. "Metallurgical effects on impact loaded materials." Shock waves and high-strain-rate phenomena in metals. Springer, Boston, MA, 1981. 325-337.

[20] Chen, Roa Wen, and K. S. Vecchio. "Microstructural characterization of shear band formation in Al-Li alloys." Le Journal de Physique IV 4.C8 (1994): C8-459.

[21] Beatty, John H., Lothar W. Meyer, Marc A. Meyers, and Sia Nemat-Nasser. "Formation of controlled adiabatic shear bands in AISI 4340 high strength steel. " No. MTL-TR-90-54. Army Lab Command Watertown Ma Material Technology Lab, 1990.

[22] Meyers, M. A., G. Subhash, B. K. Kad, and L. Prasad. "Evolution of microstructure and shear-band formation in α-hcp titanium." Mechanics of Materials17.2-3 (1994): 175-193.

[23] Xue, Qing. Spatial evolution of adiabatic shear localization in stainless steel, titanium, and Ti-6A1-4V alloy. University of California, San Diego, 2001.

[24] Meyer, L. W., and L. Krüger. "Shear testing with hat specimen." ASM Handbook, Mechanical Testing and Evaluation, ASM International, Materials Park, Ohio 8 (2000): 451-452.

[25] Wen, Chang-Da, and Issam Mudawar. "Emissivity characteristics of polished aluminum alloy surfaces and assessment of multispectral radiation thermometry (MRT) emissivity models." International journal of heat and mass transfer 48.7 (2005): 1316-1329.

[26] Mills, Kenneth C. Recommended values of thermophysical properties for selected commercial alloys. Woodhead Publishing, 2002.